

UC Davis

UC Davis Previously Published Works

Title

Contactless measurement of the photovoltage in BiVO₄ photoelectrodes

Permalink

<https://escholarship.org/uc/item/8zh5w7ms>

Journal

Energy & Environmental Science, 16(10)

ISSN

1754-5692

Authors

Daemi, Sahar

Kundmann, Anna

Becker, Kathleen

et al.

Publication Date

2023-10-11

DOI

10.1039/d3ee02087h

Peer reviewed

Contactless Measurement of the Photovoltage in BiVO₄ Photoelectrodes

Sahar Daemi,^a Anna Kundmann,^a Kathleen Becker,^a Peter Cendula,^b Frank E. Osterloh,^{*,a}

^a Department of Chemistry, University of California, Davis, CA 95616, USA
(fosterloh@ucdavis.edu)

^b Faculty of Electrical Engineering and Information Technology, University of Žilina, Liptovsky Mikulas, 03104, Slovakia

ABSTRACT

The power output of photoelectrochemical devices for solar energy-to-fuel conversion is determined by the photovoltage of the junction under illumination. In the presence of fast redox couples, the photovoltage can be obtained directly from current-voltage measurements of the device. However, for slow redox couples (H^+/H_2 , O_2/H_2O) used in solar fuel photoelectrodes, photovoltage measurements are not straightforward, due to the kinetic overpotentials during charge transfer. Here we show that the photovoltage of BiVO₄ electrodes in contact with fast electron donors KI, Na₂SO₃ or H₂O₂ or K₄Fe(CN)₆ can be measured in a contactless way with vibrating Kelvin probe surface photovoltage (SPV) spectroscopy. The photovoltage varies with illumination wavelength and intensity and matches the open circuit potential of the electrodes, obtained separately from electrochemical measurements. Plots of the photovoltage versus irradiance can be used to predict the oxidizing power of each electrode under zero applied bias. Except for K₄Fe(CN)₆, which causes shunting in the BiVO₄ electrode, photovoltage values correlate well with the built-in potential of each junction. The ability to obtain photovoltage information through contactless SPV measurements will be useful in the search for solid-liquid junctions with superior energy conversion properties.

INTRODUCTION

Photoelectrochemical devices for solar energy to fuel conversion, including photoelectrodes and photocatalysts, rely on the reactions of photogenerated charge carriers with redox species in the electrolyte. To drive a reduction or oxidation reaction, the electrochemical potential at the working electrode needs to exceed the standard reduction potentials of the acceptors or donors (e.g. 0.0 V for proton reduction or 1.23 V for water oxidation). Semiconductor electrodes promote these processes by generating a photovoltage V_{Ph} under illumination. The photovoltage corresponds to the difference of the electrochemical potentials at the back ($E_{F,b}$) and front ($E_{F,f}$) of the illuminated semiconductor – liquid junction, as shown in **Figure 1a** and **b**.¹⁻⁵ For a photoelectrode with ideal contacts (no recombination, hole or electron selectivity) the photovoltage V_{Ph} can approach the quasi-Fermi Level splitting energy (qFLS = $E_{F,n} - E_{F,p}$).⁶⁻⁸ Here $E_{F,n}$ and $E_{F,p}$ are the quasi-Fermi levels of the free electron and hole concentrations of the semiconductor in quasi-equilibrium with the exciting light source.⁹⁻¹² However, this situation is rarely approached in real photoelectrodes, where the $E_{F,n}$ and $E_{F,p}$ potentials are modified at the interfaces by the selectivity of charge transfer and by electron-hole recombination.¹⁻³

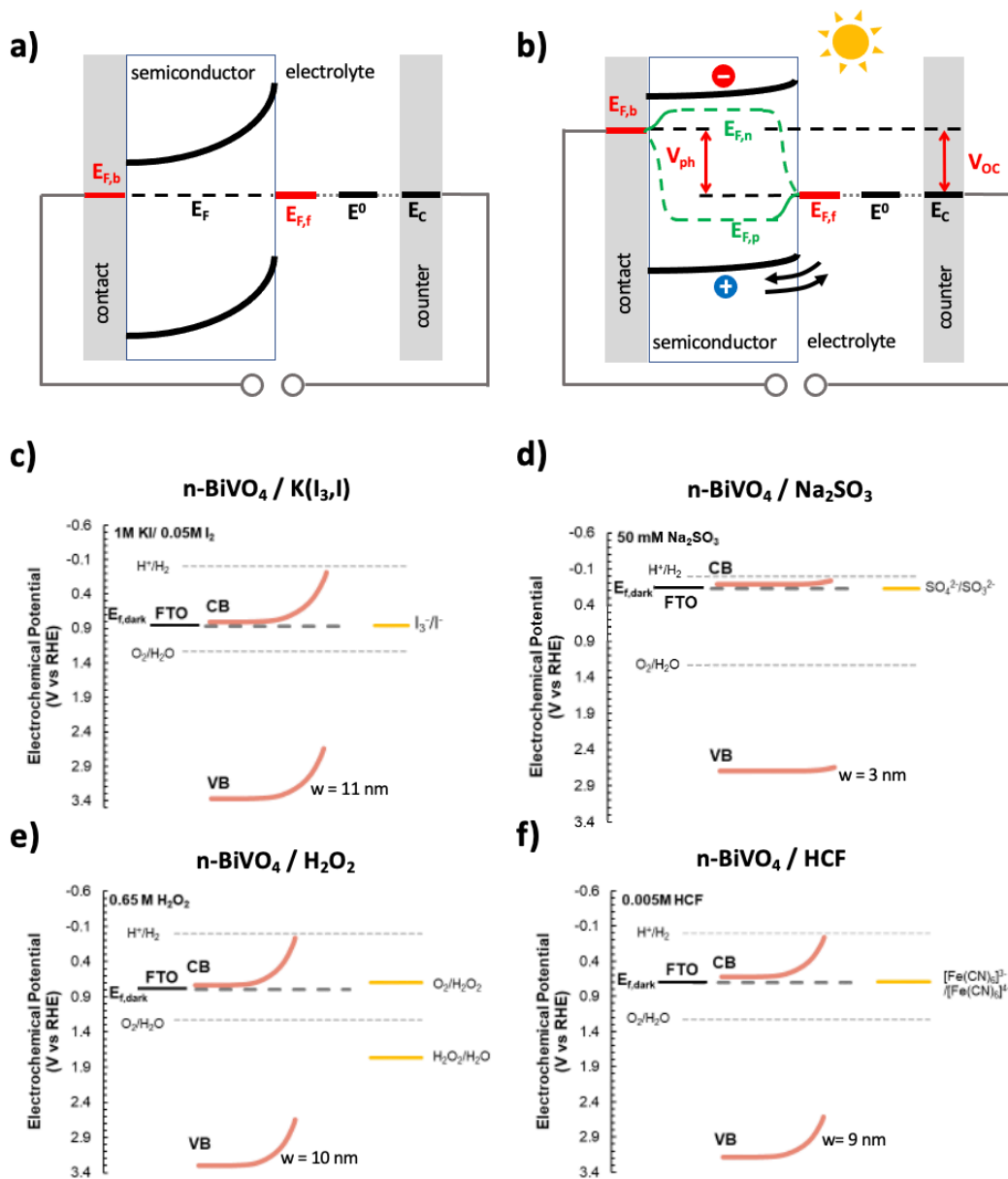


Figure 1. Energy diagram for n-semiconductor – liquid photoelectrochemical cell with a fast redox couple. a) In the dark the redox couple is in electrochemical equilibrium with the semiconductor and the counter electrode, so that $E_{F,b} = E_{F,f} = E^0 = E_C$. b) Under illumination the Fermi Levels split to produce the photovoltage, $V_{Ph} = (E_{F,b} - E_{F,f})/e$, where e is the electron charge, and $E_{F,f}$ and $E_{F,b}$ are the Fermi levels at the front and back of the semiconductor. The quasi-Fermi levels $E_{F,n}$ and $E_{F,p}$ are shown also. c-f) Band energy diagrams for BiVO_4 /liquid junctions in the dark. c) $n\text{-BiVO}_4/\text{K}(\text{I}_3, \text{I})$, d) $\text{BiVO}_4/\text{Na}_2\text{SO}_3$, e) $\text{BiVO}_4/\text{H}_2\text{O}_2$, f) BiVO_4/HCF ($\text{K}_3\text{Fe}(\text{CN})_6/\text{K}_4\text{Fe}(\text{CN})_6$). w = calculated space charge layer width. Numerical data in **Table S1**.

In semiconductor photoelectrodes with fast and reversible redox couples, V_{Ph} can be obtained from open circuit voltage (V_{OC}) measurements. This works because such redox couples are in electrochemical equilibrium with $E_{F,f}$ of the semiconductor (**Figure 1a and 1b**). However, this condition is no longer fulfilled for slow redox couples (H^+/H_2 , H_2O/O_2 , CO_2/CH_3OH) encountered in photoelectrosynthetic cells for the production of solar fuels. The slow charge transfer kinetics of these redox couples cause kinetic overpotential losses that are difficult to quantify because they depend on the electrode material, the photocurrent and other factors.^{3, 13} For example, IrO_x has a water oxidation overpotential of 0.32 V,¹³ whereas for Au_2O_3 it is 0.95 V¹⁴ (both at 10.0 mA cm⁻²). This makes it impossible to obtain the electrochemical potential $E_{F,f}$ from standard photoelectrochemical measurements. In order to measure $E_{F,f}$ in these cases, electric contact to the semiconductor-liquid junction is required. For example, Lobato et al.⁸ and Zhang et al.,¹⁵ measured the qFELS in dye-sensitized photoanodes after thermally evaporating a Ti foil electrode onto the porous TiO_2 layer. Boettcher and coworkers observed the electrochemical potential of the hematite photoelectrode surface by adding a porous gold film to it.^{16, 17} Alternatively, potential-sensing electrochemical atomic force microscopy was employed to measure the electrochemical potential at silicon/nickel/liquid interfaces,^{18, 19} and recently at illuminated $BiVO_4$ /polymer interfaces.²⁰

Here we demonstrate an alternative, contact-less, non-invasive, and simple method for the determination of V_{Ph} and $E_{F,f}$ in illuminated photoelectrodes. The approach employs Vibrating Kelvin Probe Surface Photovoltage Spectroscopy (VKP-SPS) as a highly sensitive technique (**Figure 2**) to observe photochemical charge separation in semiconductor thin films.²¹⁻²³ In VKP-SPS the contact potential difference (CPD) of a light-responsive material is measured with a

commercially available (*Besocke Delta Phi*) semitransparent gold Kelvin probe placed 1.0 - 2.0 mm above the sample. Illumination changes the charge carrier distribution to produce a surface photovoltage, $SPV = CPD(light) - CPD(dark)$. The wavelength dependence of the SPV signal, its size, sign, and reversibility, contain information about the sample band gap, the majority carrier type, the depletion layer, and defects.²⁴⁻²⁸ The method is complementary to Kelvin Probe Force Microscopy (KPFM), which measures the surface photovoltage signal with an Atomic Force Microscopy (AFM) tip.²²

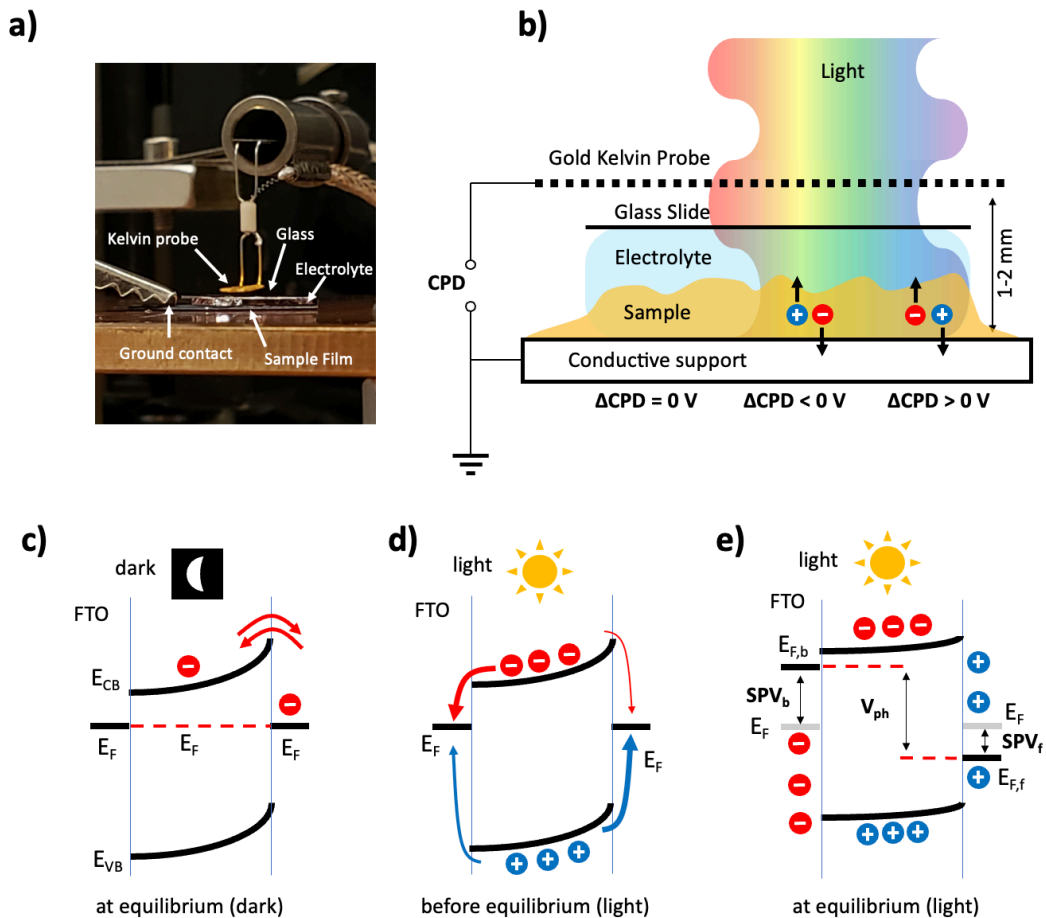


Figure 2. a) Vibrating Kelvin Probe Surface Photovoltage (VKP-SPV) Spectroscopy in liquids (Photo.) b) Schematic of the measurement configuration. Sample illumination occurs through the 60% semi-transparent KP, placed 1-2 mm above the sample, and through the electrolyte, enclosed by a microscopy glass cover slide. A water-saturated gas environment serves to prevent drying out of the electrolyte. The Contact Potential Difference (CPD) change under

illumination equals the surface photovoltage signal $SPV = CPD(\text{light}) - CPD(\text{dark})$. c) Energetics and charge carrier dynamics of a n-semiconductor-liquid junction at equilibrium in the dark, d) upon illumination, e) at quasi-equilibrium under illumination. The scheme assumes that other contributions to the SPV signal (intra-molecular charge separation, photoinduced molecular adsorption / desorption, etc.) can be neglected. ²¹

Inspired by Bastide et al's work in 1999 ²⁹ we constructed the measurement configuration in **Figure 2a** to measure SPV for *semiconductor-liquid* contacts. Here, the electrically grounded light-sensitive sample is covered by a drop of the liquid electrolyte and a microscopy cover glass slide. The Kelvin probe is then positioned about 1.0 mm over the glass surface, and the sample is illuminated through the Kelvin probe. Under these conditions, the SPV signal is generated by charge carrier separation at the semiconductor-solution interface (**Figure 2b**) and directly corresponds to the photovoltage of the semiconductor-liquid junction. ²¹⁻²³ The formation of the SPV signal can be quantitatively understood with the energy schemes in **Figure 2c-e**. In the dark, the Fermi level of the semiconductor is in electrochemical equilibrium with its interfaces at the back contact and the electrolyte. Illumination disrupts this equilibrium through production of photogenerated carriers. Transfer of the charge carriers to the back and front contacts is driven thermodynamically by the electrochemical potential gradients in the semiconductor and at its interfaces (**Figure 2d**). This produces the SPV signal with components SPV_b and SPV_f at the back and front, respectively, as defined in **equations 1** and **2**.

$$SPV_b = -(CPD_{b,fin} - CPD_{b,ini}) = -\frac{E_{F,b} - E_F}{e} \quad (\text{Eq. 1})$$

$$SPV_f = CPD_{f,fin} - CPD_{f,ini} = \frac{E_{F,f} - E_F}{e} \quad (\text{Eq. 2})$$

$$SPV = SPV_b + SPV_f = \frac{E_{F,f} - E_{F,b}}{e} = V_{Ph} \quad (\text{Eq. 3})$$

At quasi-equilibrium (**Figure 2e**) the electrochemical potentials of the back contact and the semiconductor-liquid interface equal $E_{F,b}$ and $E_{F,f}$, respectively, and the SPV signal corresponds to V_{Ph} (**equation 3**).

In order to verify **equation 3** experimentally, we performed SPV and V_{OC} measurements for n-BiVO₄ photoelectrodes immersed in solutions of various fast redox couples. For these fast redox couples, the open circuit potential V_{OC} is expected to equal the photovoltage V_{Ph} of each junction (See **Figure 1b**). Thus, a comparison of the SPV signal to V_{OC} allows us to test **equation 3**. Full details on the outcome of the measurements are presented in the following.

RESULTS AND DISCUSSION

Based on their electronic properties (**Table S1**) n-BiVO₄ electrodes are expected to form a depletion layer when in contact with aqueous redox couples with standard reduction potentials oxidizing relative to the n-BiVO₄ flatband potential. The resulting band energy schemes are shown in **Figure 1c-f** for BiVO₄ in contact with aqueous solutions of K(I₃,I), Na₂SO₃, H₂O₂, and iron hexacyanoferrate (II and III) (HCF). Built-in potentials vary between 0.17 V for the SO₄²⁻/SO₃²⁻ redox couple, to 0.89 V for the I₃⁻/I⁻ couple and depletion layers between 3 and 11 nm, respectively. Based on these energy diagrams, all BiVO₄ electrodes are expected to function as a photoanode under illumination.

SPV spectra acquired for a FTO deposited n-BiVO₄ film exposed to vacuum or aqueous KI/KI₃ solution are presented in **Figure 3a**. A negative surface photovoltage (SPV) signal forms when the photon energy approaches the band gap of BiVO₄ (2.40 eV), in agreement with the energy scheme

in **Figure 2c-e**. In vacuum (**Figure 2a**) the SPV spectrum is noisy and the SPV signal is small (-0.10 V) because the depletion layer is not yet fully formed. The addition of the KI/KI₃ electrolyte increases the SPV to values of -0.40 to -0.44, depending on the concentration. This is due to improved photohole transfer at the solid-liquid junction in **Figure 1c**. Strong SPV signals above the BiVO₄ band gap are also seen with aqueous Na₂SO₃ and H₂O₂ solutions electron donors, but not with K_{3/4}[Fe(CN)₆](aq), due to reasons discussed further below.

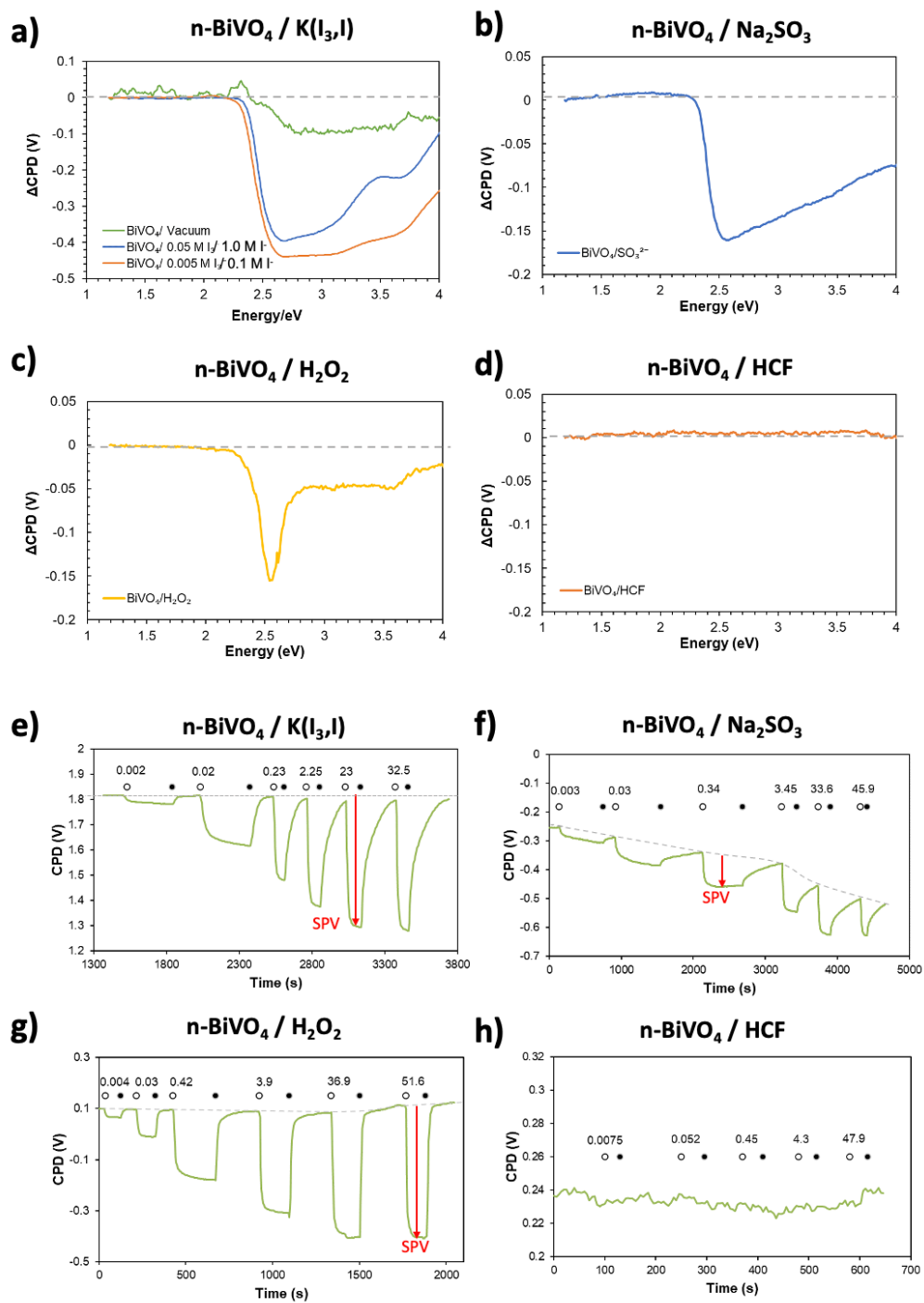


Figure 3. Surface photovoltage (SPV) spectra of a) BiVO₄ film on FTO in vacuum, or in contact with aqueous solutions of KI/KI₃, b) Na₂SO₃, c) H₂O₂, or d) K_{3/4}[Fe(CN)₆] (HCF). e-h) Surface photovoltage data under monochromatic illumination of variable irradiance (mW cm⁻²). BiVO₄ film on FTO in contact with aqueous solutions of e) KI/KI₃ (470 nm), f) Na₂SO₃ (400 nm), g) H₂O₂ (400 nm), or h) K_{3/4}[Fe(CN)₆] (HCF) (400 nm). Empty circles are

light and filled circles are dark periods. $SPV = CPD(\text{light}) - CPD(\text{dark})$. Baseline drift is attributed to charge trapping at the solid-liquid interface. Repeat measurements and statistics are shown in **Figure S3** and **Table S4**.

The shape of the spectra is modulated by the intensity output of the Xe lamp,²⁸ which causes a decay of the SPV signal above 3.6 eV, and, in the case of **Figure 3b** by the irreversible redox oxidation of sulfite, as discussed further below. Changes in the SPV spectra for the two $K(I_3, I)$ solutions are a result of competing light absorption (shading) by the I_3^- ion, which absorbs light at $\lambda < 450$ nm.³⁰

According to the Shockley diode equation (below), the open-circuit voltage of an illuminated diode increases with the logarithm of the absorbed light intensity.^{1, 3} Therefore, to quantitatively correlate the SPV signal with the photoelectrochemical properties of each junction, SPV measurements on the $BiVO_4$ liquid electrolyte configurations were repeated under 400 nm LED illumination with varied intensity (**Figure 3e-h**). For the n- $BiVO_4$ / $K(I_3, I)$ system (**Figure 3e**), a 470 nm LED was used to minimize the effect of shading by the I_3^- ion. For this system, SPV signals under 32.5 mW cm^{-2} illumination form within seconds of light exposure ($\tau_{\text{on}} = 10$ s) and decay back to baseline over the course of minutes ($\tau_{\text{off}} = 61$ s) when the light is turned off. The slower τ_{off} is due to charge transfer occurring by diffusion whereas charge separation (τ_{on}) occurs by drift in the electric field in the depletion layer. The return to baseline shows that photochemical charge separation in this system is reversible without notable charge trapping.

A different behavior is seen for the n- $BiVO_4$ film in contact with $Na_2SO_3(aq)$. Here the SPV signal is smaller, less reversible, and the baseline drifts to more oxidizing CPD values over the course of the experiment. This smaller SPV signal is due to the smaller built-in potential of the junction (0.07 V in **Table S1**), whereas the low reversibility and the baseline drift to more oxidizing values indicate the accumulation of photoholes near the $BiVO_4$ /liquid interface. This is a result of the

irreversibility of sulfite oxidation under these conditions.³¹ Larger and more reversible SPV signals are seen with H₂O₂, due to the larger built-in voltage of the n-BiVO₄/H₂O₂ junction and because of the fast electron transfer to O₂ (from H₂O₂ oxidation). No SPV signal is observed for the n-BiVO₄/HCF system, even at the highest light intensities. This is attributed to the fast reaction kinetics of the [Fe(CN)₆]^{3-/4-} redox couple, which promote back electron transfer from BiVO₄ or the FTO substrate to the oxidized [Fe(CN)₆]³⁻ ion. Shunting of metal oxide photoelectrodes with hexacyanoferrate has been previously observed with BiVO₄³² and with Fe₂O₃ photoelectrodes.³³ and is promoted by pinholes in the porous BiVO₄ film. Based on repeat measurements in **Figure S3** the SPV data is reproducible with a 6% standard deviation at the highest intensities. Standard deviations reach up to 67% for the BiVO₄/Na₂SO₃ system (**Figure S3 and Table S4**), as a result of baseline shifts associated with the irreversible charge transfer properties of the SO₄²⁻/SO₃²⁻ redox couple.

According to the diagram in **Figure 1b**, for these fast redox reagents, the photovoltage V_{ph} equals the open circuit potential (OCP) for semiconductor-liquid junctions. To verify that, OCP measurements were conducted for the four junctions in the dark and under variable light intensity (**Figure S5**). In the dark, the Fermi levels of all electrodes equal the electrochemical potential of the redox couples, in agreement with the band energy diagrams in **Figure 1**. For the BiVO₄/H₂O₂ electrode, E_F (0.80 V RHE) is found 0.105 V positive of the H₂O₂ oxidation potential (0.695 V RHE). This shows that E_F is controlled in part by the H₂O₂/H₂O (1.78 V RHE) and O₂/H₂O (1.23 V RHE) redox couples, whose standard reduction potentials are much more positive. Under illumination, all photoanodes generate cathodic Fermi level shifts from the transfer of

photoelectrons toward the FTO/BiVO₄ interface. The largest potential changes (>0.60 V) are seen for BiVO₄/K(I₃,I) and the smallest (<0.04 V) for BiVO₄/HCF.

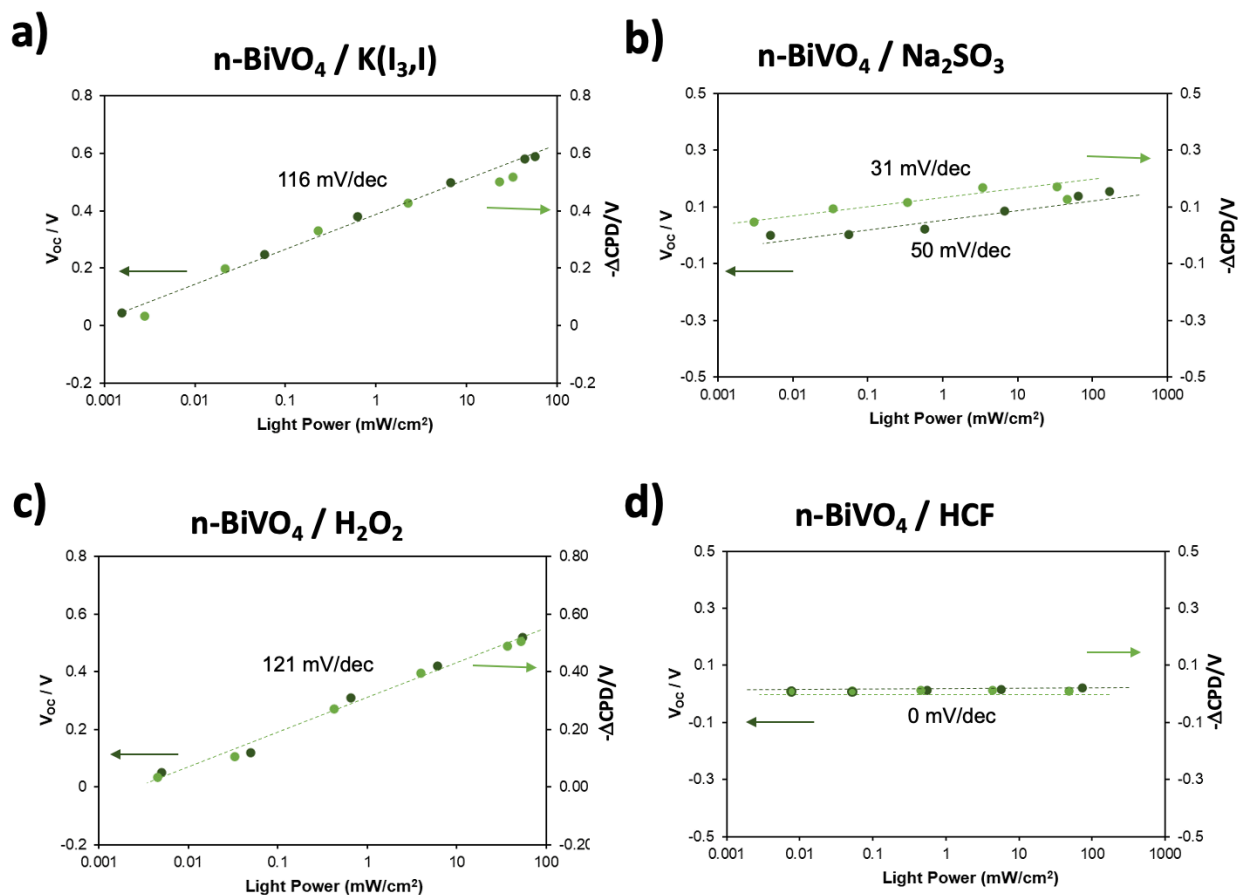


Figure 4. Open circuit potentials (V_{oc}) and $-\Delta CPD$ values versus logarithmic irradiance ($mW\ cm^{-2}$). V_{oc} values were calculated from the data in **Figure 3** and **S5** using **equation 4**.

From the $E_{F,b}$ and E_F values in **Figure S5**, the open circuit voltage V_{oc} of each electrode can be calculated with **equation 4**.

$$V_{oc} = E_{F,b} - E_F \text{ (dark)} \quad (\text{Eq. 4})$$

Figure 4 plots the V_{OC} data and the SPV data versus the logarithm of the irradiance. With $K(I_3, I)$, H_2O_2 , and HCF electrolytes, V_{OC} values and SPV values are nearly identical over the entire irradiance range. This is an important confirmation of **equation 3**. For Na_2SO_3 , SPV values are found to be ~ 100 mV larger than V_{OC} values. This discrepancy arises because of the irreversible redox chemistry of the SO_4^{2-}/SO_3^{2-} redox couple under the measurement conditions. Because SO_4^{2-} cannot accept electrons from $BiVO_4$, positive charge (protons from $2 h^+ + SO_3^{2-} + H_2O \rightarrow SO_4^{2-} + 2 H^+$) builds up at the $BiVO_4$ /electrolyte interface. This shifts the E_F level to more oxidizing values after each illumination cycle as can be seen in the SPV baseline shift (0.25 V) in **Figure 3f** and in the OCP baseline shift (0.07 V) in **Figure S5b**. **Equation 4** does not capture this E_F variation and therefore underestimates the V_{OC} values by 0.07-0.25 V. As a result, the SPV values in **Figure 8b** are a more reliable descriptor of the open-circuit voltage of the $BiVO_4/Na_2SO_3$ contact.

The Shockley diode equation (**equation 5**)³⁴⁻³⁶ predicts a linear increase of SPV and V_{OC} values versus the logarithmic irradiance.* The data in **Figure 4** mostly conforms to the equation. Deviations from linearity at higher light intensity for the V_{OC} with Na_2SO_3 are attributed to the irreversibility of sulfite oxidation, as discussed above.

$$V_{OC} = n \frac{kT}{e} \ln \left(\frac{j_{phot}}{j_0} + 1 \right) \quad (\text{Eq. 5})$$

For ideal junctions, the open-circuit voltage increases by 59 mV for every decadic increase of the irradiance, corresponding to a diode ideality factor $n=1$. However, solid-liquid junctions in photoelectrochemical cells are rarely ideal because the built-in potential changes with the chemical

* In the equation, k, T and e have their usual meanings, and j_{phot} and j_0 are the photocurrent density and reverse bias current density of the junction

composition and oxidation state of the interface.^{16, 37} Indeed, experimental slopes for KI and H₂O₂ are 116 - 121 mV dec⁻¹, corresponding to ideality factors of 2.0 - 2.1, while the small slope of 31 mV dec⁻¹ for Na₂SO₃ corresponds to $n = 0.5$. These deviations from ideality are due to the irreversibility of the SO₄²⁻/SO₃²⁻ redox couple under these conditions³⁸ and due to the multi-electron redox chemistry of H₂O₂ and iodide oxidation.

Using the intensity-dependent V_{Ph} and $E_{F,b}$ data, the absolute electrochemical potential $E_{F,f}$ at the semiconductor-liquid interface can be calculated from **equation 3**. All E_F values are plotted versus the logarithmic irradiance in **Figure 5**.

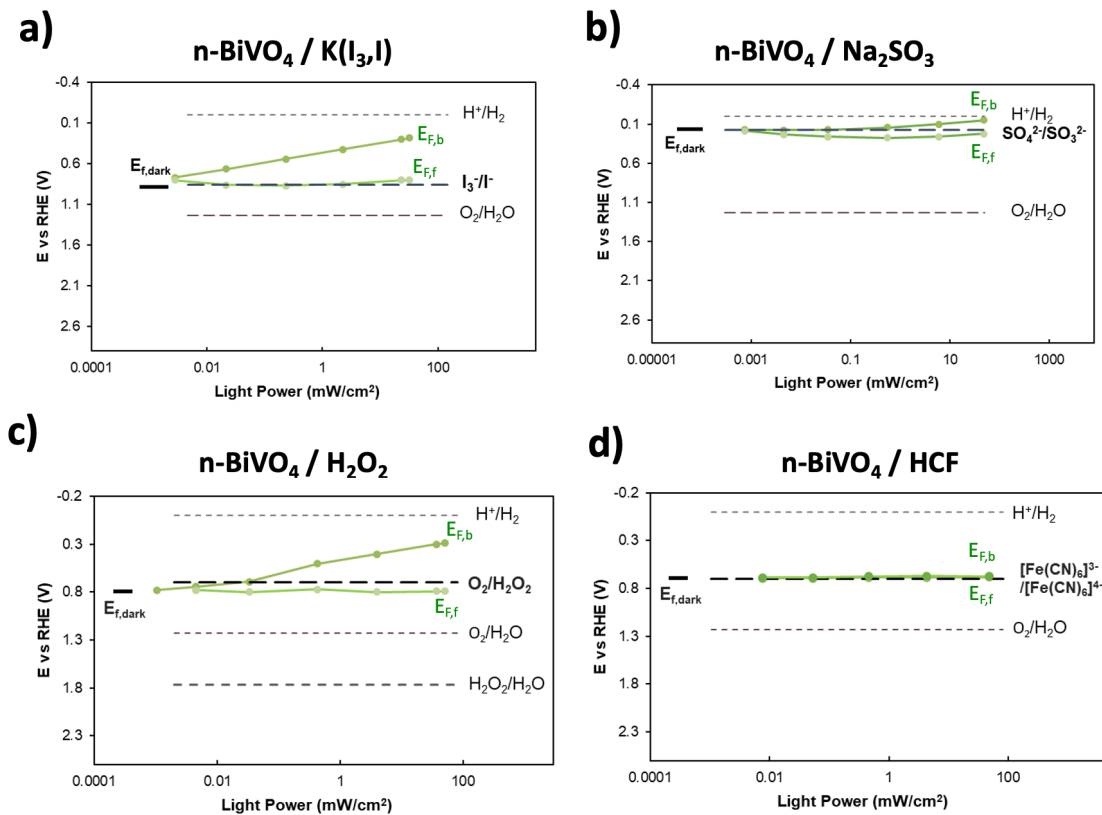


Figure 5. Plots of Fermi Levels $E_{F,b}$ and $E_{F,f}$ versus logarithm of irradiance. $E_{F,b}$ values are from open circuit potential measurements in **Figure S5** and $E_{F,f}$ values were calculated from SPV data using **equation 3**.

In the dark, the $E_{F,f}$ values of all electrodes are controlled by the electrochemical potentials of the redox couples. Illumination with increasing light intensity moves $E_{F,b}$ to reducing potentials, whereas $E_{F,f}$ values remain near the E^0 solution potential. This confirms that the position of $E_{F,f}$ is controlled by the electrochemical potential of the redox couples, as expected for these fast hole acceptors.^{38, 39} $E_{F,f}$ for $\text{SO}_4^{2-}/\text{SO}_3^{2-}$ is ~ 0.1 V more oxidizing than the E^0 value for this redox couple. This is a result of the irreversible redox chemistry of sulfite, which leads to positive charge accumulation at the $\text{BiVO}_4/\text{liquid}$ interface, and a corresponding shift of $E_{F,f}$ to more oxidizing values. Comparing $E_{F,f}-E_{F,b}$ differences at equal irradiance of 15 mW cm^{-2} , $\text{K}(\text{I}_3,\text{I})$ enables the largest open-circuit voltage (0.50 V), followed by $\text{O}_2/\text{H}_2\text{O}_2$ (0.44 V), and $\text{SO}_4^{2-}/\text{SO}_3$ (0.17 V). This trend follows the relative sizes of built-in potentials with KI (0.79 V), H_2O_2 (0.7 V), Na_2SO_3 (0.07 V) (**Table S1** and **Figure 4**). Larger built-in potentials enable better hole selectivity and lower electron-hole recombination. Despite the large band bending ($V_{\text{bi}}=0.60$ V, see **Table S1**), the BiVO_4/HCF system does not produce a photovoltage because of back electron transfer via the BiVO_4 conduction band or the FTO back contact.

Based on the Fermi level plots in **Figure 5**, BiVO_4 photoanodes should be able to oxidize Na_2SO_3 , H_2O_2 , and KI without applied bias, but not HCF. To test this prediction, short circuit current measurements with a Pt counter electrode were conducted. The results in **Figure S6** show that indeed, large short-circuit current (I_{SC}) of $>0.90 \text{ mA cm}^{-2}$ for the $\text{BiVO}_4/\text{K}(\text{I}_3,\text{I})$ system and of 2.5 mA cm^{-2} for the $\text{BiVO}_4/\text{H}_2\text{O}_2$ junction can be obtained. For the latter, O_2 gas evolution is observed at the BiVO_4 electrode (**Figure S1c**), confirming that the current is from H_2O_2 oxidation. Similar gas bubbles are also seen at the end of the SPV experiment (**Figure S1b**). The relatively small short-circuit current (I_{SC}) of $\sim 32 \text{ } \mu\text{A cm}^{-2}$ for the $\text{BiVO}_4/\text{Na}_2\text{SO}_3$ system is a result of the small open-circuit voltage of this junction. As expected, no photocurrent is seen with HCF because of

shunting. Overall, the photocurrent data confirms the validity of the quasi-Fermi Level plots in **Figure 5**.

CONCLUSION

In summary these first Vibrating Kelvin Probe Surface Photovoltage (VK-SPV) measurements on BiVO₄ in contact with liquid electrolytes show that the SPV signal equals the photovoltage (V_{Ph}) of each electrode. V_{Ph} values depend on illumination wavelength and irradiance, as predicted by the Diode equation. By combining the V_{Ph} data with open circuit potential measurements, the electrochemical potentials $E_{\text{F},\text{f}}$ at the front of the photoelectrodes can be estimated. We find that $E_{\text{F},\text{f}}$ values are ‘pinned’ to the electrochemical potential of the respective redox couples because of rapid hole transfer from BiVO₄. Except for $[\text{Fe}(\text{CN})_6]^{3-/4-}$, which causes shunting, the V_{Ph} values correlate well with the built-in voltage V_{bi} of each system. This confirms V_{bi} as an important predictor of the energy conversion efficiency of BiVO₄ photoelectrodes. Because the VKP-SPV technique is non-destructive and non-invasive, it should be of significant value in the search for new photoelectrodes and photocatalysts for the conversion of solar energy into fuels and electricity.

CONFLICTS OF INTEREST

There are no conflicts of interest to declare.

EXPERIMENTAL SECTION

Bismuth(III) nitrate pentahydrate (99.999 %, Acros Organics), Nitric acid (70.0 %, Sigma-Aldrich), Vanadyl acetylacetonate (99%; Acros Organics), Dimethyl sulfoxide ($\geq 99.9\%$; Sigma-Aldrich), P-benzoquinone ($\geq 98\%$; Sigma-Aldrich), Potassium iodide (99.0%; Merk), Iodine ($\geq 99.8\%$; Sigma-Aldrich), Sodium sulfate ($\geq 99.0\%$; Sigma-Aldrich), Potassium hexacyanoferrate(II) trihydrate (98.5-102.0%; Sigma-Aldrich), Potassium ferricyanide (99.2%; Sigma-Aldrich), Sodium sulfite ($\geq 98\%$; Sigma-Aldrich), Sodium sulfite ($\geq 98\%$; Sigma-Aldrich), Potassium phosphate monobasic (98%; Sigma-Aldrich), Hydrogen peroxide (30% aqueous solution, by weight; Sigma-Aldrich), Sodium hydroxide ($\geq 97\%$; Sigma-Aldrich), were used as-received.

n-BiVO₄ films were prepared on fluorine doped tin oxide (FTO) by electrochemical deposition of BiOI followed by reaction with VO(acac)₂ at 450 °C according to Kyoung-Shin Choi's method and etching in 1.0 M NaOH solution.³⁹

Surface photovoltage (SPV) data was obtained with the vibrating Kelvin probe technique, using a semi-transparent (60%) 3.0 mm diameter gold Kelvin probe (*Kelvin Probe S, Delta PHI Besocke*) and a *Besocke Kelvin Control*. Measurements were conducted in a custom-made chamber under vacuum ($\leq 2 \times 10^{-4}$ mbar) or in H₂O-saturated N₂ gas. Samples were coated with 10-15 μ L of liquid electrolytes using a micropipette and covered with a glass cover slip (Fisher Scientific, 0.17 to 0.25 mm thickness). For the acquisition of full spectra, samples were illuminated through the Kelvin probe using light from a 300 W Ce lamp filtered through an Oriel Cornerstone 130 monochromator (1-10 mW cm⁻²). Scans were performed from 9600 cm⁻¹ to 40000 cm⁻¹ by stepping

the photon energy by 0.0124 eV every 5 s and by measuring the contact potential difference (CPD) value at each step. The light exiting the monochromator had a FWHM (full-width/half-maximum) of 8 nm–15 nm, depending on the wavelength, and an average intensity of 50 $\mu\text{W}/\text{cm}^2$ in the 2.0 eV–3.6 eV interval. The contact potential difference (CPD) data were corrected for drift effects by subtracting a fitted logarithmic curve of a dark scan from the spectral scan.

Intensity-dependent measurements were performed with air-cooled 400 nm or 470 nm LED arrays connected to a DC power supply. The voltage was regulated to produce irradiances of 5×10^{-4} – 60 mW/cm^2 at the sample surface, as measured by a photometer equipped with a GaAsP UV-Vis detector (International Light Technologies, Inc), and after correction using a 60% transmission value for the Kelvin probe.

Open circuit potential (OCP) measurements were conducted with a Gamry Reference 600 potentiostat in a two-electrode system consisting of the sample as working electrode and a calomel electrode (3.5 M KCl) as counter electrode. All electrolytes were purged with N_2 for 20 min before and during the measurements, except for H_2O_2 solutions, which were left open to air. The cell was calibrated using the standard reduction of potential of hexacyanoferrate (0.358 V vs NHE) and potentials were then adjusted to the RHE scale using the formula $V_{\text{RHE}} = V_{\text{NHE}} + 0.0592 \times \text{pH}$. Illumination was provided by 400 nm or 470 nm LEDs.

Chronoamperometry scans were performed in a 2-electrode set-up, with the sample as the working electrode and a Pt wire as both the counter and reference electrode. For H_2O_2 short circuit photocurrent measurement, a graphite electrode was used as both the counter and reference electrode to avoid H_2O_2 disproportionation. A 0 V bias was applied and a 400 nm or 470 nm LED was used as the light source.

Electrolytes were prepared as follows: 1.0 M phosphate buffer stock solution (PBS) at pH 6.66 was prepared by dissolving 3.40 g KH_2PO_4 in 250 mL of water, followed by adjusting the pH to 6.66 with 2M KOH solution. 0.05 M PBS was prepared by diluting the stock solution and by adjusting the pH further with 2.0 M KOH to 6.66. pH was measured with a pH meter (Fisher Scientific *Accumet* AE150). 0.05 M Na_2SO_3 in 0.1M Na_2SO_4 was prepared by adding 0.630 g Na_2SO_3 to 100 mL of 0.1M Na_2SO_4 (0.05 M Na_2SO_3 pH=9.58). 5 mM HCF in 0.1M Na_2SO_4 was prepared by adding 0.0739 g of $\text{K}_4\text{Fe}(\text{CN})_6$ and 0.0576 g of $\text{K}_3\text{Fe}(\text{CN})_6$ to 35 mL of 0.1 M Na_2SO_4 (5 mM HCF pH=5.6). 0.65 M H_2O_2 in 0.1M Na_2SO_4 was prepared by adding 2.0 mL of a 30% aqueous H_2O_2 to 28 mL of 0.1 M Na_2SO_4 (0.65 M H_2O_2 pH=4.21). 0.05 M triiodide solution in 0.05 M PBS was prepared by making a 95%/5% molar ratio between KI and I_2 solutions. For that, 1.0 M KI/0.05 M I_2 was prepared by adding 1.66 g of KI and 0.128 g of I_2 to 0.05 M PBS. 10 times diluted solution was prepared by preparing 0.1M KI/5 mM I_2 through adding 0.166 g of KI and 0.0128 g of I_2 to 0.05 M PBS.

ACKNOWLEDGEMENT

The authors thank the U.S. Department of Energy, Office of Science, Office of Basic Energy Sciences under Award Number DOE-SC0015329 for financial support of this work. P.C. thanks Slovak Research and Development Agency under contract APVV-20-0528 and support of the project Innovative Solutions for Propulsion, Power and Safety Components of Transport Vehicles, ITMS 313011V334. We would like to express our special gratitude to Dr. Thomas Dittrich for insightful discussions.

AUTHOR CONTRIBUTIONS

The experiments were designed by F.E.O and S.D. and conducted by S.D. The manuscript was written by F.E.O and S.D. with contributions by A.K, K.B., and P.C. All authors have given approval to the final version of the manuscript.

SUPPORTING INFORMATION

The following supporting information is available: Selected Semiconductor Data, Photos of the Photoelectrodes, Open Circuit Potential Data, Short Circuit Photocurrent Data.

DATA AVAILABILITY

Data will be made available at the UC Davis University Repository at <https://datadryad.org> and can be downloaded using the following link: <https://doi.org/10.25338/B83H0K>

REFERENCES

1. P. Würfel, *Physics of Solar Cells*, Wiley-VCH, Weinheim, 2005.
2. U. Würfel, A. Cuevas and P. Würfel, *IEEE Journal of Photovoltaics*, 2015, **5**, 461-469.
3. R. Memming, in *Semiconductor Electrochemistry*, 2015, DOI: <https://doi.org/10.1002/9783527688685.ch7>, pp. 169-266.
4. R. Krol, *Photoelectrochemical Hydrogen Production*, 2012, **102**, 13-67.
5. A. J. Bard, R. Memming and B. Miller, *Pure and Applied Chemistry*, 1991, **63**, 569-596.
6. M. X. Tan, C. N. Kenyon and N. S. Lewis, *Journal of Physical Chemistry*, 1994, **98**, 4959-4962.
7. O. Kruger, C. N. Kenyon, M. X. Tan and N. S. Lewis, *Journal of Physical Chemistry B*, 1997, **101**, 2840-2849.
8. K. Lobato, L. M. Peter and U. Würfel, *The Journal of Physical Chemistry B*, 2006, **110**, 16201-16204.
9. W. Shockley and H. J. Queisser, *J. Appl. Phys.*, 1961, **32**, 510-519.
10. H. Gerischer, *J. Electroanal. Chem.*, 1977, **82**, 133-143.
11. P. Würfel, *Journal of Physics C: Solid State Physics*, 1982, **15**, 3967.
12. J. Faisst, M. List, F. Heinz and U. Würfel, *Advanced Optical Materials*, 2022, **10**, 2200909.
13. C. C. L. McCrory, S. H. Jung, J. C. Peters and T. F. Jaramillo, *J. Am. Chem. Soc.*, 2013, **135**, 16977-16987.
14. O. Diaz-Morales, F. Calle-Vallejo, C. de Munck and M. T. M. Koper, *Chemical Science*, 2013, **4**, 2334-2343.

15. S. Zhang, X. Yang, K. Zhang, H. Chen, M. Yanagida and L. Han, *Physical Chemistry Chemical Physics*, 2011, **13**, 19310-19313.
16. F. D. Lin and S. W. Boettcher, *Nature Mater.*, 2014, **13**, 81-86.
17. M. R. Nellist, F. A. L. Laskowski, F. Lin, T. J. Mills and S. W. Boettcher, *Accounts of Chemical Research*, 2016, **49**, 733-740.
18. M. R. Nellist, F. A. L. Laskowski, J. Qiu, H. Hajibabaei, K. Sivula, T. W. Hamann and S. W. Boettcher, *Nature Energy*, 2018, **3**, 46-52.
19. F. A. L. Laskowski, S. Z. Oener, M. R. Nellist, A. M. Gordon, D. C. Bain, J. L. Fehrs and S. W. Boettcher, *Nature Mater.*, 2020, **19**, 69-76.
20. M. Shen, A. J. Kaufman, J. Huang, C. Price and S. W. Boettcher, *Nano Lett.*, 2022, **22**, 9493-9499.
21. T. Dittrich and S. Fengler, *Surface Photovoltage Analysis of Photoactive Materials*, World Scientific Publishing Europe Ltd., London, 2020.
22. R. Chen, F. Fan, T. Dittrich and C. Li, *Chem. Soc. Rev.*, 2018, **47**, 8238-8262.
23. L. Kronik and Y. Shapira, *Surf. Sci. Rep.*, 1999, **37**, 1-206.
24. L. Barnea-Nehoshtan, S. Kirmayer, E. Edri, G. Hodes and D. Cahen, *The Journal of Physical Chemistry Letters*, 2014, **5**, 2408-2413.
25. S. Rühle and D. Cahen, *Journal of Applied Physics*, 2004, **96**, 1556-1562.
26. L. Burstein, J. Bregman and Y. Shapira, *Journal of Applied Physics*, 1991, **69**, 2312-2316.
27. R. M. Doughty, B. Hodges, J. Dominguez, R. Han, Z. Zhao, S. Assavachin and F. E. Osterloh, *The Journal of Physical Chemistry C*, 2020, **124**, 18426-18435.

28. R. M. Doughty, F. A. Chowdhury, Z. Mi and F. E. Osterloh, *The Journal of Chemical Physics*, 2020, **153**, 144707.
29. S. Bastide, D. Gal, D. Cahen and L. Kronik, *Review of Scientific Instruments*, 1999, **70**, 4032-4036.
30. J. M. Gardner, M. Abrahamsson, B. H. Farnum and G. J. Meyer, *Journal of the American Chemical Society*, 2009, **131**, 16206-16214.
31. S. C. Yen and T. W. Chapman, *Journal of The Electrochemical Society*, 1985, **132**, 2149.
32. B. Zhang, X. Zhang, X. Xiao and Y. Shen, *ACS Appl. Mater. Interfaces*, 2016, **8**, 1606-1614.
33. B. M. Klahr and T. W. Hamann, *J. Phys. Chem. C*, 2011, **115**, 8393-8399.
34. M. X. Tan, P. E. Laibinis, S. T. Nguyen, J. M. Kesselman, C. E. Stanton and N. S. Lewis, *Progress in Inorganic Chemistry, Vol 41*, 1994, **41**, 21-144.
35. R. Memming, in *Electron Transfer I*, 1994, vol. 169, pp. 105-181.
36. P. Salvador, *J. Phys. Chem. B*, 2001, **105**, 6128-6141.
37. D. E. Aspnes and A. Heller, *J. Phys. Chem. C.*, 1983, **87**, 4919-4929.
38. N. Buhler, K. Meier and J. F. Reber, *J. Phys. Chem.*, 1984, **88**, 3261-3268.
39. T. W. Kim and K.-S. Choi, *Science*, 2014, **343**, 990-994.